Title

Growth monitoring of field-grown onion and garlic by CIE L*a*b* color space and region-based crop segmentation of UAV RGB images

Authors

Kim, Dong-Wook
Jeong, Sang Jin
Lee, Won Suk
et al.

Publication Date

2023

DOI

10.1007/s11119-023-10026-8

Precision Agriculture
https://doi.org/10.1007/s11119-023-10026-8

Growth monitoring of field-grown onion and garlic by CIE L*a*b* color space and region-based crop segmentation of UAV RGB images

Dong-Wook Kim[1,2] · Sang Jin Jeong[1] · Won Suk Lee[3] · Heesup Yun[4] · Yong Suk Chung[5] · Young-Seok Kwon[6] · Hak-Jin Kim[1,2,7]

Accepted: 20 April 2023

Abstract
Canopy coverage-based crop growth monitoring is highly dependent on the performance of crop segmentation algorithms. Under field conditions, crop segmentation for unmanned aerial vehicle (UAV) imagery should be sophisticated considering geometric distortion of images by wind and illumination variations. Under Korean cultivation conditions, a plastic mulch used to restrict weeds and prevent cold weather damage increases the complexity of the image background. In particular, on-site monitoring of onion and garlic growth has been limited by their morphology because they have long narrow leaves. The ultimate goal of this study was to quantify the growth parameters of onion and garlic at multiple growth stages using red, green, and blue (RGB) imagery obtained with UAVs. Canopy coverage and plant height were used as predictor variables to develop mathematical models to estimate the fresh weights of onion and garlic. The use of a CIE L*a*b* color space and mean shift (MS) algorithm enhanced the extraction of the canopy coverage of onion and garlic from complex backgrounds, including plastic mulch, soil, and shadows under varying illumination conditions. Multiple linear regression models consisting of the a* band-based vegetation fraction (VF) and structure from motion (SfM)-based plant height (PH) fitted the fresh weight data of onion and garlic well with high coefficients of determination (R^2) ranging from 0.82 to 0.92. The validation results showed an almost 1:1 slope with highly linear relationships ($R^2 > 0.82$) between the onion and garlic fresh weights obtained with the UAV RGB imagery and actual fresh weights, confirming that the UAV-RGB imagery based on the use of the a*band and PH can be used to quantify the spatial and temporal variability of onion and garlic growth parameters during the growing season.

Keywords Unmanned aerial vehicle · Crop segmentation · CIE L*a*b* color space · Crop with long narrow leaves · Growth monitoring · Remote sensing

✉ Hak-Jin Kim
kimhj69@snu.ac.kr

Extended author information available on the last page of the article

Published online: 11 May 2023

Introduction

Field crop growth monitoring plays a crucial role in assessing overall crop health, determining irrigation timing, and estimating potential yields (Hunt et al., 2010). Periodic monitoring of biophysical parameters such as biomass, leaf area index (LAI), vegetation index (VI), and plant height (PH) can assist growers in successfully optimizing inputs like fertilizers and pesticides, as well as properly forecasting final harvests (Borchard et al., 2015; Dammer et al., 2009; Thorp et al., 2012). Traditional crop monitoring studies have used field measurements or aerial/satellite data to cover large areas effectively. Field-based methods including in situ sampling and laboratory analysis are often destructive, labor-intensive, costly, and time-consuming, thereby limiting the number of samples required for an effective crop growth management setup (Chang et al., 2011).

Precision agriculture is a site-specific soil and crop management system that uses various engineering technologies, such as the global navigation satellite system (GNSS), geographic information systems (GIS), and remote sensing (RS), to assess variability in soil properties (e.g., pH, organic matter, and soil nutrient levels), geographic condition (e.g., slope and elevation), and crop parameters (e.g., yield and biomass) (Kim et al., 2018). Recently, unmanned aerial vehicles (UAVs) have become increasingly popular for low-altitude and high-resolution remote sensing applications due to their benefits for precision agriculture, which include adaptability, lightweight, and low operating costs. UAV systems have become a cost-effective, novel remote sensing platform due to advancements in the precision, economic efficiency, and downsizing of numerous technologies such as global positioning system (GPS) receivers and computer processors (Holman et al., 2016). UAV imagery can be used to assess crop growth conditions including canopy greenness, leaf area, water stress estimation, and various geographical circumstances such as crop area, digital surface models (DSMs), and depth contour lines (Salamí et al., 2014; Zhang & Kovacs, 2012).

In UAV remote sensing-precision agriculture, detecting canopy coverage in crops is an essential step before addressing further objectives such as calculating the percentage of green cover and predicting yields (Hernández-Hernández et al., 2016; Torres-Sánchez et al., 2015). In particular, the canopy coverage commonly represents the growth status of crops and yields in the regions of interest in remote sensing. Canopy coverage is needed to estimate fresh weight (Kim et al., 2018), plant height (Fernández-Pacheco et al., 2014), and yield (Hernández-Hernández et al., 2016; Torres-Sánchez et al., 2015). In addition, for root crops such as onion, garlic, white radish, canopy coverage is related to root depth (Escarabajal-Henarejos et al., 2015). Crop segmentation techniques for canopy coverage calculation have gained importance and have been developed for various purposes (Hernández-Hernández et al., 2016; Łuszczkiewicz-Piątek, 2014). Under field conditions, crop segmentation must be sophisticated, considering atmospheric interference, daily illumination intensities, and complex backgrounds. Recently, many studies have been conducted for precision agriculture to accurately separate crops using various image processing algorithms based on UAV imagery (Liu et al., 2022; Osco et al., 2021; Shao et al., 2022). In addition, many studies have been conducted on plant detection and counting (Bai et al., 2022; Tu et al., 2020; Valente et al, 2020), and growth estimation (Costa et al., 2022; Fei et al., 2022; Xu et al., 2022) by applying image processing algorithms suitable for various environments.

For crop segmentation, the color feature is one of the most widely used visual features in image retrieval because of its robustness, effectiveness, and computational simplicity

(Hong et al., 2004; Sarkate et al., 2013). Many studies on the VI, such as excess green (ExG) (Woebbecke et al., 1995), excess red (ExR) (Meyer et al., 1999), and normalized differential index (NDI) (Hunt et al., 2005) have been conducted for crop segmentation. These indices are widely used to separate soil and plant pixels. ExG, which can separate vegetation in backgrounds with soil, straw, and stones in outdoor conditions, is the most commonly used VI in UAV-remote sensing and growth modeling studies. Furthermore, Otsu's thresholding method, which is an automatic thresholding method, is simple and performs well on images that can be divided into two classes (Otsu, 1979). Many researchers have used ExG-Otsu's thresholding method for crop segmentation techniques. However, crop segmentation is difficult because crop color changes easily depending on the imaging sensor, crop morphology, and illumination conditions in the outdoor field. Moreover, shadows and interreflection under field conditions also cause illumination complexities. In this regard, ExG-Otsu's thresholding method for crop segmentation has not been verified under various illumination conditions.

Onion (*Allium cepa*) and garlic (*Allium sativum*) are vegetables that are commonly cultivated and used in various dishes and seasonings and are also among the main ingredients of kimchi in Korea. Onion and garlic are root crops, unlike wheat, barley, and maize, and the health of the leaves at the early growth stage has a substantial influence on yield because nutrients from leaves at the early growth stage migrate to roots at the mid and late-growth stages (Lopez-Bellido et al., 2016). Therefore, for both onion and garlic, canopy coverage is a crucial factor for the evaluation of crop growth conditions and accurate measurement of canopy coverage is needed for indirectly monitoring other growth factors such as fresh weight, root weight, plant height, and yield.

However, accurate measurement of canopy coverage for onion and garlic is difficult because they are crops with long narrow leaves. In crops with long narrow leaves, the boundary between the crops and background is long and complex compared to those without such leaves. Therefore, it is difficult to recognize the boundary between the crops and background in the image, and the latter is greatly affected by shadows and light conditions. In addition, because the leaves are narrow, the number of pixels recognized as leaves is small, so the image resolution is greatly affected when separating the crops from the background. Under Korean cultivation conditions, plastic mulch is commonly used to restrict weeds and prevent cold weather damage to onion and garlic. This complicates image analysis since it is much more difficult to separate crops from plastic mulch than from soil because images of crops on plastic mulch are highly affected by shadows and light reflections. There have been a few studies on the segmentation of crops with long narrow leaves, and particularly, there is scarce research conducted on onion and garlic in Korean cultivation conditions. Thus, research on the separation of crops with long narrow leaves on plastic mulch is challenging but necessary for applying precision agriculture in Korean cultivation conditions.

Furthermore, the atmosphere and sunlight affect the images acquired by UAVs more than those taken with ground vehicles. Even after radiometric calibration, which is applied in UAV remote sensing, illumination variation occurs within the whole field image, resulting in poor quality crop segmentation if soil and vegetation are separated by a single threshold value. Thus, the use of a VI-based method that is sensitive to light conditions, such as the ExG-Otsu's thresholding method, may be limited for segmenting crops with long narrow leaves on plastic mulch, using UAV imagery.

To overcome the disadvantages of the ExG-Otsu method, some studies have attempted to perform segmentation using image processing in other color spaces. For example, when using the HSV (hue, saturation, and value) color space or the CIE L*a*b* (L*: lightness,

a*: green–red, b*: blue–yellow) color space, these color spaces have been proven to prevent inaccurate segmentation caused by shading, overexposure, and underexposure (Riehle et al., 2020). The CIELAB color space, also referred to as L*a*b*, is a color space defined by the International Commission on Illumination (abbreviated CIE) in 1976. CIELAB was intended as a perceptually uniform space, where a given numerical change corresponds to a similar perceived change in color. In particular, the CIE L*a*b* color space is a color model that was proposed based on how colors are organized and conceptualized in human vision in terms of other color attributes such as lightness, hue, and the RGB color model. These color spaces have the advantage of representing the color of a pixel in channels separated from the brightness. Some previous works (Bai et al., 2014; Hamuda et al., 2017) found that grayscale values converted from RGB values did not produce adequate segmentation performance, thus motivating the use of the CIE L*a*b* color space in agriculture. These studies have shown that incorrect segmentation caused by shadows, overexposure, and underexposure can be reduced with these color spaces.

In our previous study (Kim et al., 2018), the ExG-Otsu thresholding algorithm was applied to separate Chinese cabbage (*Brassica rapa* subsp. *pekinensis*) and white radish (*Raphanus sativus*) from the background to model and monitor the biophysical parameters of the crops. The ExG-Otsu algorithm showed segmentation performance of over 85% to be used for monitoring Chinese cabbage and white radish, but there was no report on the performance of crops with relatively long narrow leaves such as onion and garlic.

In this regard, the overall goal of this study was to investigate the potential of using UAV-based RGB imagery to effectively monitor temporal and spatial variability during the growth stage and quantify the growth parameters of onion and garlic cultivated in agricultural fields. The first specific objective was to develop a robust crop segmentation algorithm for onion and garlic with long narrow leaves under complex illumination and background conditions and compare the performance of the developed algorithm with that of the previous segmentation method (Kim et al., 2018). The performance of the algorithms was evaluated by comparison to that obtained using manual method. The second specific objective was to generate statistical models to quantify the growth parameters of onion and garlic based on the use of the newly developed crop segmentation algorithm, and investigate the applicability of the developed models using additional field experiment in the same field but re-cultivated in the following year.

Materials and methods

Test plot

A two-year field experiment was conducted during the 2017 and 2018 growing seasons, from March to April. UAV remote sensing for image acquisition was conducted in an onion and garlic field of the Bioenergy Crop Research Institute (35° 03′ N, 126° 22′ E, altitude 12 m), located in 199 Muan-ro, Muan gun, Jeollanam-do, Republic of Korea (Fig. 1). Data obtained from the 2017 field experiment were used to develop statistical models that could quantify the growth parameters of onion and garlic. Testing was performed using data obtained from the 2018 experiment to validate the developed regression models. White plastic mulch films were used to suppress weed growth before planting in both years. Fifty-five-day-old onion (*Allium cepa*) seedlings were planted on 25 October 2016, and 5

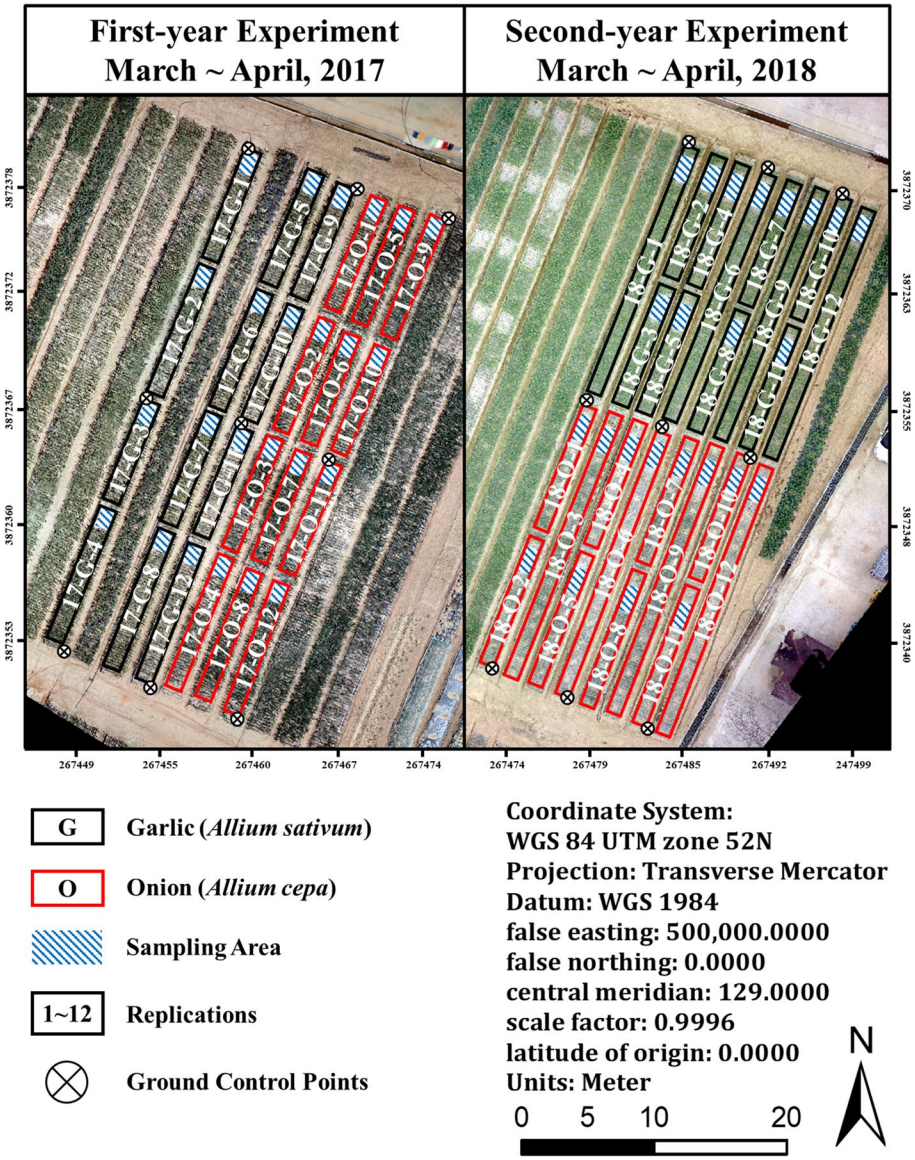

Fig. 1 Test sites during the 2017 and 2018 onion and garlic growing seasons

November 2017. Garlic (*Allium sativum*) seeds were planted on 25 September 2016, and 5 October 2017.

UAV flight and image acquisition

A hexarotor airframe model (F550, DJI Innovations, Shenzhen, China) served as the aerial platform to acquire images. The UAV was set to automatically fly over the fields using

an automatic flight controller (Pixhawk, 3D Robotics, Berkeley, CA, USA). The Mission Planner program (ArduPilot Development Team and Community) was used to track waypoints according to the pre-programmed flight path generated. An RGB commercial camera (S110, Canon, Tokyo, Japan) was attached to the UAV as the image sensor. The sensor resolution of the camera was set to 12 megapixels (4000 × 3000 pixels) to achieve a ground resolution of approximately 3.7 mm pixel^{-1} at a flight altitude of 10 m. The actual size of a frame on the ground was approximately 40 × 15 m. From a preliminary test to determine the appropriate camera parameters for decreasing image blur, the shutter speed and F-stop (aperture) were set at 1/2000s and 4.0, respectively, with the focus distance set at infinity. A summary of the flight missions is provided in Table 1.

In each mission, aerial images were captured at a scheduled flight altitude of 10 m with an intended overlap of 70% to ensure image redundancy. The Pix4Dmapper Pro 3.0.17 software (Pix4D SA, Lausanne, Switzerland), which allows image mosaicking, was used to generate a complete crop map of the total study area. Similar to what was reported in a previous study (Turner et al., 2012), to improve the spatial accuracy of the aerial imagery obtained by the UAV, nine ground control points (GCPs) consisting of 0.3 × 0.3 m paper sheets were placed at the corners and center of the test plot. The GCP locations were measured using a Novatel OEM 615 virtual reference station (VRS)-based real-time kinematic (RTK)-GPS to provide positioning accuracy within 20 and 50 mm in the horizontal and vertical directions, respectively. All images containing GPS information were aligned and converted into an orthomosaic in Pix4Dmapper Pro 3.0.17. The growth stages of onion and garlic were determined according to the "Biologische Bundesanstalt, Bundessortenamt und CHemische Industrie" (BBCH) scale, which is used to identify the phenological development stages of plants (Lancashire et al., 1991).

To perform statistical analysis of the UAV images and ground truth data for onion and garlic, 1.2 × 1.2 m regions of interest (ROIs) representing the area of each grid were used. Approximately 64 plants were included in each ROI because onion and garlic were grown at a plant spacing of 0.13 m. To obtain actual data on growth parameters (i.e., top weight and root weight) for each crop, 10 plants located in each ROI were randomly removed from the field and investigated after every UAV flight. The ten plant samples were collected

Table 1 UAV imaging details and BBCH code of onion and garlic used in the 2017 and 2018 growing seasons

Date	BBCH code		Flight altitude (m)	Ground resolution (mm pixel^{-1})	Flight time	Illumination	Wind (m s^{-1})
	Onion	Garlic					
24/03/2017	19	19	10	3.7	10–11 am	Cloudy	2.0
04/04/2017	41	41	10	3.7	11 am–12 pm	Clear sky	2.1
14/04/2017	43	43	10	3.7	10–11 am	Cloudy	5.2
28/04/2017	47	47	10	3.7	11 am–12 pm	Clear sky	3.1
14/03/2018	15	17	10	3.7	1–2 pm	Cloudy	3.5
23/03/2018	19	19	10	3.7	12–1 pm	Clear sky	2.6
30/03/2018	41	41	10	3.7	11 am–12 pm	Clear sky	1.9
13/04/2018	43	43	10	3.7	11 am–12 pm	Cloudy	3.5
20/04/2018	45	45	10	3.7	12–1 pm	Clear sky	1.4
27/04/2018	47	47	10	3.7	11 am–12 pm	Clear sky	1.9

from each ROI and were weighed using an electronic scale in the laboratory. The ten values were averaged as a representative value.

Radiometric calibration

To reduce the effects of changing light and atmospheric conditions on the UAV images taken at different times, radiometric calibration was performed at each flight by placing 1.2 × 1.2 m Group 8 Technology Type 822 ground calibration panels for airborne sensors with seven grayscales (3, 5, 11, 22, 33, 44, and 55%) at a location within the flight path of the UAV platform. Radiometric calibration with empirical lines (Wang and Soe, 2015) was conducted to remove atmospheric interference with standard calibration panels as shown in Eqs. 1 and 2:

$$r_{x,k} = \frac{\int_{400}^{800} R_x(\lambda) C_k(\lambda) \mathrm{d}\lambda}{\int_{400}^{800} C_k(\lambda) \mathrm{d}\lambda} \tag{1}$$

$$r_{x,k} = A_k \exp\left(B_k * DN\right) \tag{2}$$

where $r_{x,k}$ represents the calculated mean reflectance values of the calibration targets (airborne sensor ground calibration panels, Inc. Group Eight Technology, Provo, Ut, USA), $R_x(\lambda)$ is the standard reflectance spectrum of the calibration targets, $C_k(\lambda)$ is the spectral response of the RGB camera (S110, Canon, Tokyo, Japan), A_k, B_k are the coefficients of the exponential relationship, and DN represents the digital number of the image. The detail information of radiometric calibration was described in our previous study (Kim et al., 2018).

Crop segmentation methods

Two different segmentation methods, namely a combination of the ExG and Otsu's automatic threshold, and a combination of the a* band and region-based threshold, were used to identify a method suitable for separating the onion and garlic from the background. Since ExG could effectively assess canopy variation in green crop biomass based on RGB imagery (Kim et al., 2018; Torres-Sánchez et al., 2014), ExG was calculated based on the RGB reflectance values obtained with the UAV-RGB camera, using Eq. 3 (Woebbecke et al., 1995):

$$ExG = 2g - r - b \tag{3}$$

where r is $\frac{R}{R+G+B}$, g is $\frac{G}{R+G+B}$, b is $\frac{B}{R+G+B}$, and R, G, and B represent the reflectance values of the red, green, and blue bands in the radiometrically calibrated images, respectively.

In principle, since Otsu's thresholding is used as an automatic threshold method that assumes that the image contains two classes of pixels, such as crops and other background objects, the optimum threshold can be determined based on minimizing the interclass variance and maximizing the intraclass variance (Otsu, 1979). Using Otsu's threshold, the ExG images were then converted into binary images and classified into two different groups (i.e., vegetation or background).

The other segmentation method was to use the CIE L*a*b* color space based on how colors are structured and conceptualized in human vision in terms of other color-making

qualities including lightness, hue, and the RGB color model (Riehle et al., 2020). Specifically, the a* band in the CIE L*a*b* color space was used to distinguish crops, soil, shadows, and plastic mulch because the negative a* band value is more green and its positive value is more red.

In conjunction with the use of the a* band index, a region-based mean-shift (MS) algorithm was used to solve the single peak problem of the a* band image. The MS is a nonparametric feature-space mathematical analysis technique for locating the maxima of a density function, a so-called mode-seeking algorithm (Cheng, 1995). In this study, the MS algorithm was used for thresholding a* band images by clustering the images. Clustering in the MS algorithm was performed according to the following principles: (a) Consider a set of points in a two-dimensional space, and (b) assume a circular window centered at C and having radius r as the kernel. MS is a hill-climbing algorithm that involves shifting this kernel iteratively to a higher density region until convergence is attained. Every shift is defined by a mean shift vector. The MS vector always points toward the direction of the maximum increase in density. At every iteration, the kernel is shifted to the centroid or the mean of the points within it. The method for calculating this mean depends on the choice of kernel. A flat kernel was selected in this study. At convergence, there will be no direction in which a shift can accommodate more points inside the kernel. In previous studies (Ammour et al., 2017; Yan et al., 2020), the MS algorithm has been used to conduct various image processing research such as object detection, segmentation, and tracking. In this study, the RGB image was classified into green and non-green vegetation with the a* band feature using the MS algorithm.

Histogram analysis of a garlic-field RGB image depending on the index used (i.e., ExG and a*-band indices) was performed to investigate how various objects in the garlic field affect the histogram distribution. As shown in Fig. 2, by manually plotting each object corresponding to the crop, shadow, plastic mulch, and soil in ENVI 5.4 (Harris, Broomfield, CO, USA), the histogram distribution of each component was obtained for the ExG and a* band indices. There were both wet and dry parts of crop and soil in this sample (Fig. 2). The index values of the ExG and a* band image were normalized between 0 and 255.

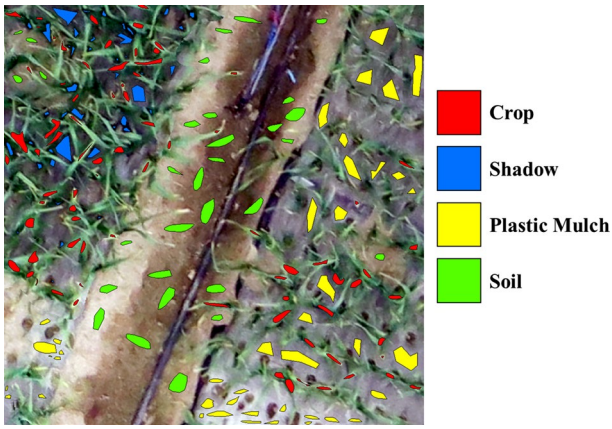

Fig. 2 Selection of regions of interest (ROIs) of various objects (crop, shadow, plastic mulch, and soil) in a garlic field image used for histogram analysis

Calculation of vegetation fraction and plant height

In accordance with the methods described by Kim et al. (2018), the vegetation fraction (VF) was used as an index to quantify the canopy coverage. The VF in each ROI was calculated as the ratio of the number of pixels segmented as a crop to the number of total pixels, using Eq. 4:

$$\text{Vegetation Fraction (VF)} = \frac{\text{Number of pixels determined as crop}}{\text{Number of total pixels}} \tag{4}$$

To evaluate the performance of the ExG with Otsu threshold algorithm and a*band with MS algorithm in terms of VF, 30 UAV RGB images from the early to late growth stages of garlic were used. The actual VF was determined by calculating the percentage of vegetation using the ENVI 5.4 program after manually delineating the vegetation in the raw image. The accuracy of the two different segmentation methods applied in the study was assessed by comparing them with manually identified actual VFs for all of the 30 sample images.

In accordance with the methods described in our previous study (Kim et al., 2018), since plant height (PH) can be used as an index of vertical crop growth, the PH was defined as the shortest distance between the upper section of the onion and garlic plants and the ground. The plants and ground were represented using the DSM and digital terrain model (DTM), respectively. That is, the DTM was defined as a model of a field without crops, whereas the DSM was a model of a field with crops.

The 3D points of the DSM and DTM were created to calculate PH using Pix4Dmapper Pro 3.0.17. The DTM was acquired on the first UAV flight, carried out within 7 days after sowing, when the crops had not yet germinated, and the DSMs were acquired on each subsequent UAV flight date. As shown in Fig. 3, the PH, defined as a field feature model only, was then calculated by subtracting the DSM from the DTM (Eq. 5):

$$\text{Plant Height} = \text{DSM} - \text{DTM} \tag{5}$$

where DSM represents the model of the underlying topography with crops, and DTM represents the underlying topography of the field without crops.

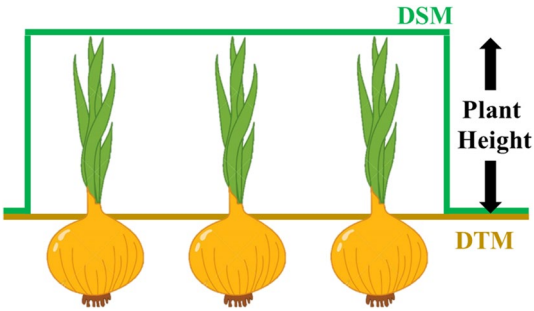

Fig. 3 Schematic of plant height (PH) calculation based on the subtraction of the digital terrain model (DTM) from the digital surface model (DSM)

Fresh weight prediction modeling and validation

Following the methods used in our previous study (Kim et al., 2018), multiple linear regression models were developed to quantify onion and garlic growth from UAV-based imagery. Predictor variables (X) were vegetation fraction (VF) and plant height (PH), and response variables (Y) were growth parameters. An interaction term of VF × PH was added to the predictor variables, as shown in the following equation (Eq. 6):

$$Y = A \times X_{VF} + B \times X_{PH} + C \times X_{VF} \times X_{PH} + D \quad (6)$$

where Y represents the fresh weights of onion and garlic, X_{VF} represents the VF variable, X_{PH} represents the PH variable, and A, B, C, and D represent the estimates of each of the predictor variable terms.

SAS 9.4 software (SAS Institute, Cary, NC, USA) was used to determine the four estimates for Eq. 6 (A–D) by fitting the image data acquired from the UAV in terms of VF and PH to the equation. Validation of the developed regression models was conducted by comparing the fresh weights estimated using the developed regression models with those measured with an electronic balance for both onion and garlic samples obtained in the following year (2018).

Results and discussion

Identification of crop segmentation method for onion and garlic

Figure 4 shows the histogram distributions and box plots for garlic and other objects in the field, corresponding to the ExG and a* band indices. As shown in Fig. 4a, since the ExG index of the crop was distributed between 84 and 255, whereas the index ranges of the shadow, plastic mulch, and soil were in the ranges of 24–255, 27–85, and 0–119, respectively, the crop showed an overlap of 84 to 119 with other objects. The ExG image showed 20% overlap between crops and other things. In addition, the shadow covered most of the index range of the ExG image from 20 to 255. Therefore, the ExG-based crop segmentation was greatly affected by shadows, implying that the use of ExG would be vulnerable to light and shadow conditions.

Figure 4b shows the histogram distribution of the a* band image. Since the index of the crop was distributed between 0 and 148 whereas the index ranges of the shadow, plastic mulch, and soil were 140–220, 103–195, and 149–255, respectively, the garlic crop was clearly distinguished from the background even though the crop and plastic were partially overlapped in the range of 103 to 148. The a* band had less overlap in vegetation and other parts of field. This result suggests that the a* band would be more applicable than ExG for the segmentation of crops with long narrow leaves, which are more vulnerable to the effects of light and shadow.

Figure 5 shows the effect of the Otsu's threshold on automatic segmentation in two different band images (ExG and a*-band indices). When the ExG and a* band images were converted into binary images (i.e., 1 or 0) using Otsu's method, the histogram distribution of the a* band was composed of a single peak (Fig. 5b), unlike the ExG, which showed two peaks (Fig. 5a). This result suggests that using the Otsu's threshold would not be suitable for crop segmentation in the a* band.

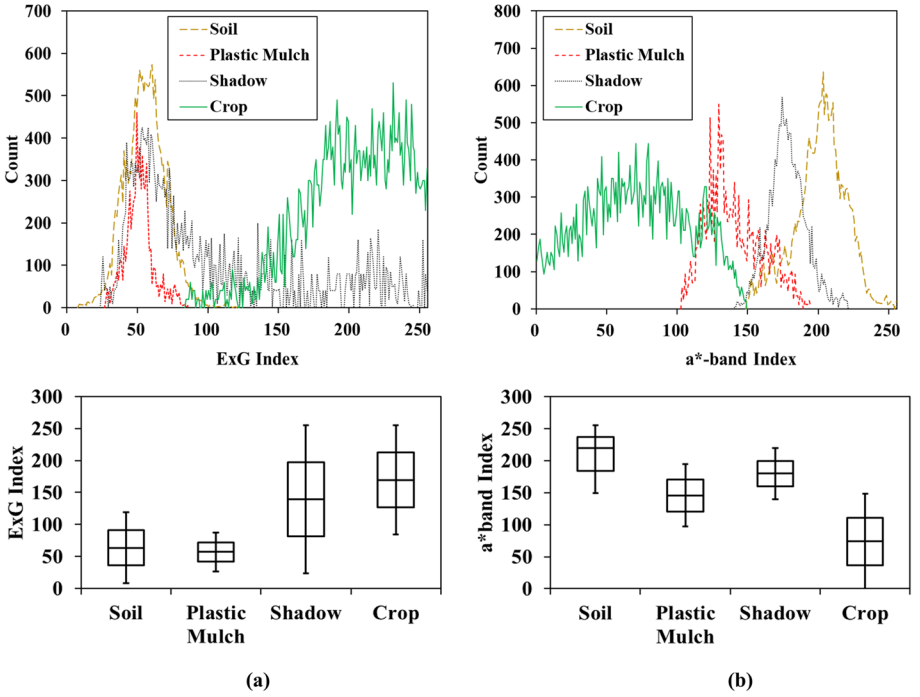

Fig. 4 Histogram distributions and box plots of garlic and other objects in the field, corresponding to the **a** excess green (ExG) and **b** a* band images

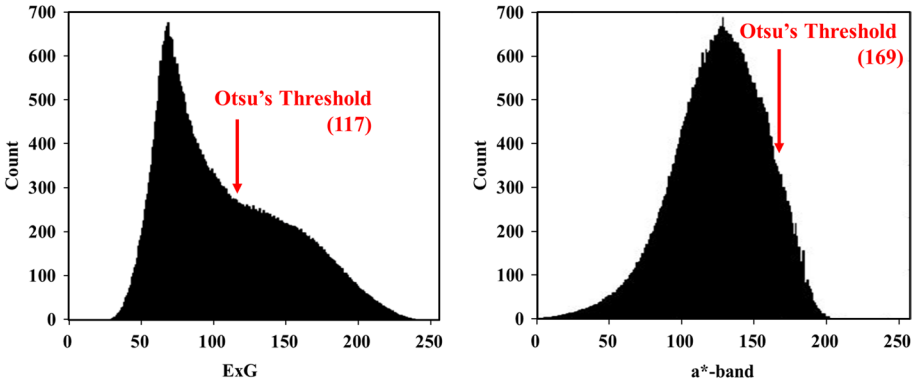

Fig. 5 Histogram distribution and Otsu's thresholding values of excess green (ExG) and a* band images for crop segmentation

In this study, the MS algorithm was used to solve the single peak problem of the a* band image. Using the MS algorithm allows for a clearer conversion from the a* band image into a binary image by creating a clustered image with a clustered histogram. Figure 6 shows details of the newly developed a* band and MS-based crop segmentation algorithm which allowed calculating the vegetation fraction. First, an RGB image (Fig. 6a) was

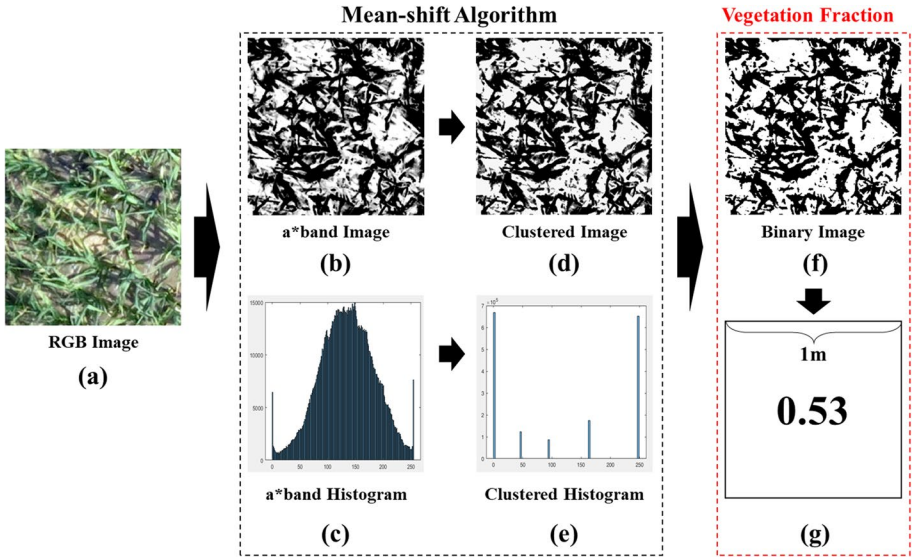

Fig. 6 The newly developed a* band and mean-shift (MS)-based crop segmentation algorithm for calculating the vegetation fraction: **a** RGB image; **b–e** MS algorithm; **f, g** vegetation fraction calculation

converted into an a* band image (Fig. 6b). Then, the a* band image (Fig. 6b) was grouped into the clustered image (Fig. 6d) using the MS clustering algorithm. The clustering result could also be confirmed by the change of the histogram. The single peak histogram of the original a* band image (Fig. 6c) was converted into a clustered histogram divided into five by the MS algorithm. Since the a* band index shows a greener color for lower values, the pixels with the lowest value among the five peaks were set as the crop. Finally, the ratio of the pixels set as the crop to the total pixels in the binary image was calculated as the vegetation fraction (Fig. 6f and g).

Figure 7 shows an example of garlic segmentation using an ExG image with Otsu's thresholding and a* band image with the MS algorithm. An RGB image was converted into an ExG image (Fig. 7b) and a CIE a* band image (Fig. 7d). When the ExG image was converted into a binary image using Otsu's thresholding, the ExG-based binary crop image was overestimated because the ExG might be greatly affected by light and shadow conditions (Fig. 7c). On the other hand, when an a* band image was converted into a binary image after the MS algorithm was applied (Fig. 7e), it was observed that the garlic crop was more clearly segmented due to the lesser effect of shadows and light compared to that obtained with Otsu's method (Fig. 7f).

Figure 8 shows a comparison of crop segmentation accuracy between the image manually segmented and that automatically segmented. The latter was obtained using a combination of ExG and Otsu's thresholding and a combination of the a* band and MS algorithm. Figure 8a shows the time-series accuracy of the algorithms according to days after transplanting (DAT). In order to calculate the average and standard deviation of accuracy (%), five randomly selected samples were used for each stage from the early and late growth stages. The ExG + Otsu's thresholding method showed low accuracy in both early and late growth stages, while the a* band + MS algorithm showed an improvement in performance over time. In the late growth stage, there were limitations of the Otsu threshold due to the abundance of crops covering the field and reducing the

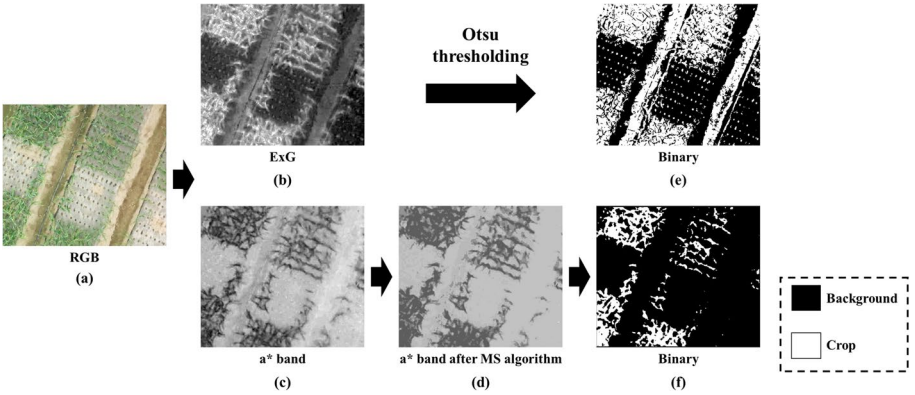

Fig. 7 An example of crop segmentation using **a, b, e** excess green (ExG) + Otsu's thresholding and **a, c, d, f** the a* band + mean-shift (MS) algorithm

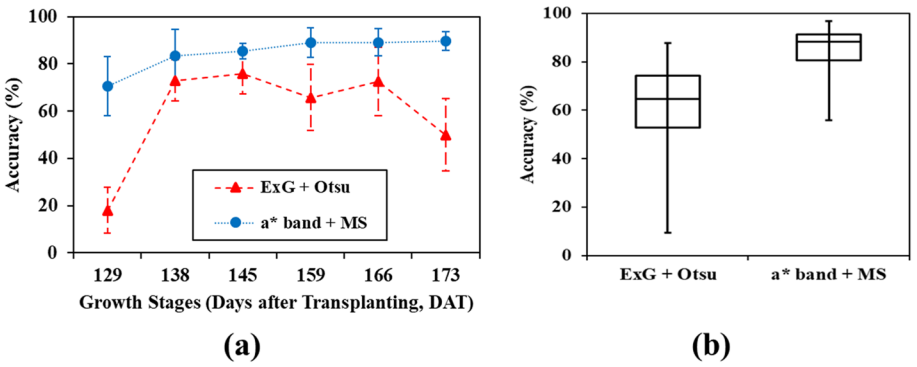

Fig. 8 Performance comparison of crop segmentation methods (Excess green + Otsu's thresholding method and a* band + mean-shift algorithm) using 30 sample images: **a** Box plots with accuracy evaluation; **b** time-series accuracy evaluation according to the days after transplanting (DAT)

background. Thus, the ExG + Otsu's thresholding method showed a high-level over-estimation in the late growth stages. On the other hand, the developed a* band + MS algorithm showed high segmentation accuracy even in the late growth stage as there was less over-estimation.

As shown in Fig. 8b, when the total 30 sample images were evaluated using the accuracy index, the average segmentation performance of the a* band + MS algorithm was 84.6%, and that of the ExG + Otsu's thresholding was 59.2%. The 15.4% error of the a* band + MS algorithm might be due to the overlap between the crop and plastic mulch in the a* band index shown in the histogram analysis (Fig. 4).

In summary, compared to ExG and Otsu's thresholding, the use of the a* band + MS algorithm enhanced the extraction of the canopy coverage of onion and garlic from backgrounds including plastic mulch, soil, and shadows under varying illumination conditions.

Onion and garlic yield modeling and validation

Table 2 shows the results of the regression analysis for modeling the growth status of the two crops, using the a* band and MS algorithm. When using four predictor variables (VF, PH, VF×PH, and constant) and two different response variables (top weight and root weight), all of the multiple regression equations based on the developed method showed coefficients of determination (R^2) between 0.82 and 0.92. In our previous study (Kim et al., 2018), when predicting growth parameters such as leaf length and fresh weight of Chinese cabbage and white radish using the ExG + Otsu thresholding method, multiple regression equations showed R^2 between 0.78 and 0.94. Therefore, it was expected that the use of the growth models based on the developed method (a* band + MS algorithm) would allow measuring the growth parameters of onion and garlic with a similar level of performance in the previous study. Thus, the developed growth models could be used as a method to predict the potential yields of the two crops before harvest.

In this study, the ground truth top and root weight of onion and garlic were compared from early to late growth stages. As a result, a high linear relationship was observed between the top and root weight of onion, showing R^2 of 0.88 with a slope of 0.75. Moreover, the top and root weight of garlic showed a high linear relationship with R^2 of 0.82 with a slope of 0.22. These results suggest that although onion and garlic are root crops, the top and root parts of the crops are highly correlated. Therefore, it was possible to estimate the root weight of the crops even by using the UAV image comprising only the above-ground data.

Validation of the developed growth estimation models for onion and garlic was performed using a different dataset of UAV images with known growth data obtained from the second-year experiment (2018). A total of 56 and 66 ROIs of onion and garlic, respectively, were used to quantify their growth parameters during the 2018 growing season.

In this study, a two-point normalization method was applied to improve the growth estimation performance of onion and garlic. The two-point normalization method is an algorithm that uses two known samples of distinct values to adjust for discrepancies in slope and offset between model estimates and actual values before analysis (Kim et al., 2013). To maximize the effect of two-point normalization employing a wide range of data, it is necessary to select two known samples with the biggest difference in growth parameters. The slope and offset were directly compensated by comparing the actual values obtained from destructive sampling and the estimated values obtained with UAV imagery on each flight. The performance of the two-point normalization method was already validated in our previous study for the growth modeling of Chinese cabbage and white radish (Kim et al., 2018).

Table 2 Results of multiple linear regression equations for estimating the growth parameters of onion and garlic based on the developed a* band + mean shift (MS) algorithm: Y = growth parameters; X_{VF} = vegetation fraction value; X_{PH} = plant height value; n = number of samples; R^2 = coefficient of determination

Crop	Growth parameter	Multiple regression models	n	R^2
Onion	Top weight (g)	$Y = 68.4 \times X_{VF} - 0.8 \times X_{PH} + 139.7 \times X_{VF} \times X_{PH} + 4.4$	42	0.92
	Root weight (g)	$Y = -5.5 \times X_{VF} - 50.5 \times X_{PH} + 241.8 \times X_{VF} \times X_{PH} + 5.7$	42	0.82
Garlic	Top weight (g)	$Y = 68.5 \times X_{VF} - 19.7 \times X_{PH} + 54.7 \times X_{VF} \times X_{PH} + 13.3$	39	0.84
	Root weight (g)	$Y = 9.9 \times X_{VF} - 7.0 \times X_{PH} + 14.9 \times X_{VF} \times X_{PH} + 5.1$	39	0.82

For instance, when applying the developed regression models (Table 2) for estimating the top and root weights of onion and garlic grown in the following year (Fig. 9a and c), the developed models performed well in estimating the top and root weight of onion, exhibiting strong linear relationships with $R^2 > 0.85$ and slopes of 1.06 and 0.87 between the developed regression models and standard methods. Similarly, as shown in Fig. 9b and d, the developed models for garlic showed strong linear relationships with $R^2 > 0.82$ and slopes of 1.02 and 1.01. The obtained validation results for onion and garlic were comparable to those obtained for Chinese cabbage and white radish. In our previous study (Kim et al., 2018), the developed models for Chinese cabbage and white radish showed linear relationships with $R^2 > 0.80$ in the validation test. The use of the a* band and MS algorithm would be satisfactory for estimating the fresh top and root weights of onion and garlic.

Spatial mapping of potential yields of onion and garlic

The UAV RGB image (Fig. 10a) obtained on April 27, 2018, was converted into a top-weight map (Fig. 10b) calculated with the developed regression models for investigating the feasibility of applying the UAV approach for mapping the onion and garlic yield potential during the growing season. Crop ROIs were made by sequentially locating each 1.2 × 1.2 m area along the planting rows in the UAV RGB image using ArcGIS 10.1. As a result, 128 and 120 ROIs were created for onion and garlic, respectively, to calculate the VF and PH values, which were then used as predictor variables to estimate the top weights of onion and garlic in each ROI. Finally, maps of each crop were

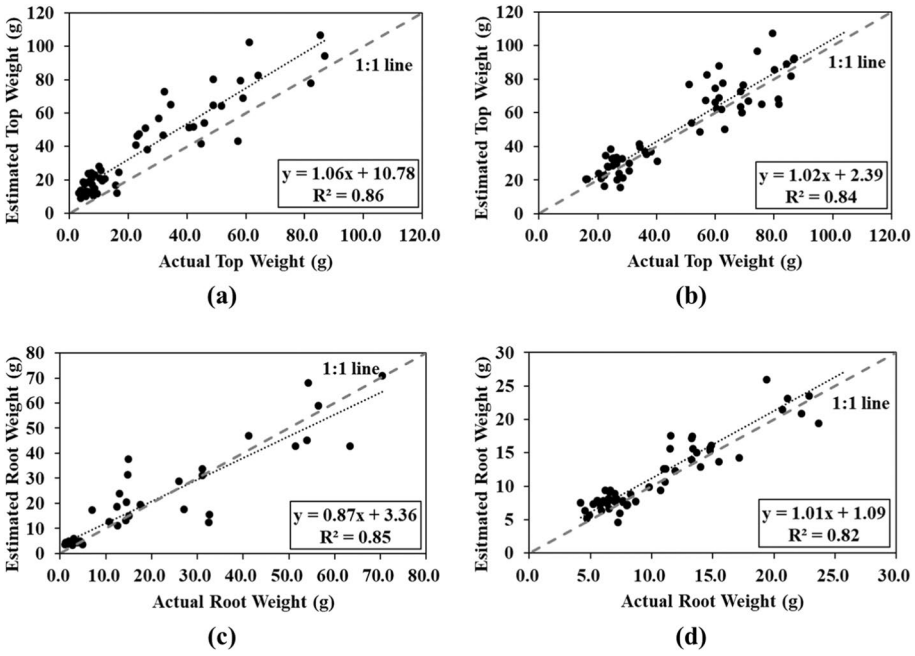

Fig. 9 Scatter plots of crop growth parameters **a, b** top weight and **c, d** root weight for **a, c** onion and **b, d** garlic using the unmanned aerial vehicle (UAV)-based images and ground truth data obtained by standard methods during the second-year (2018) experiment

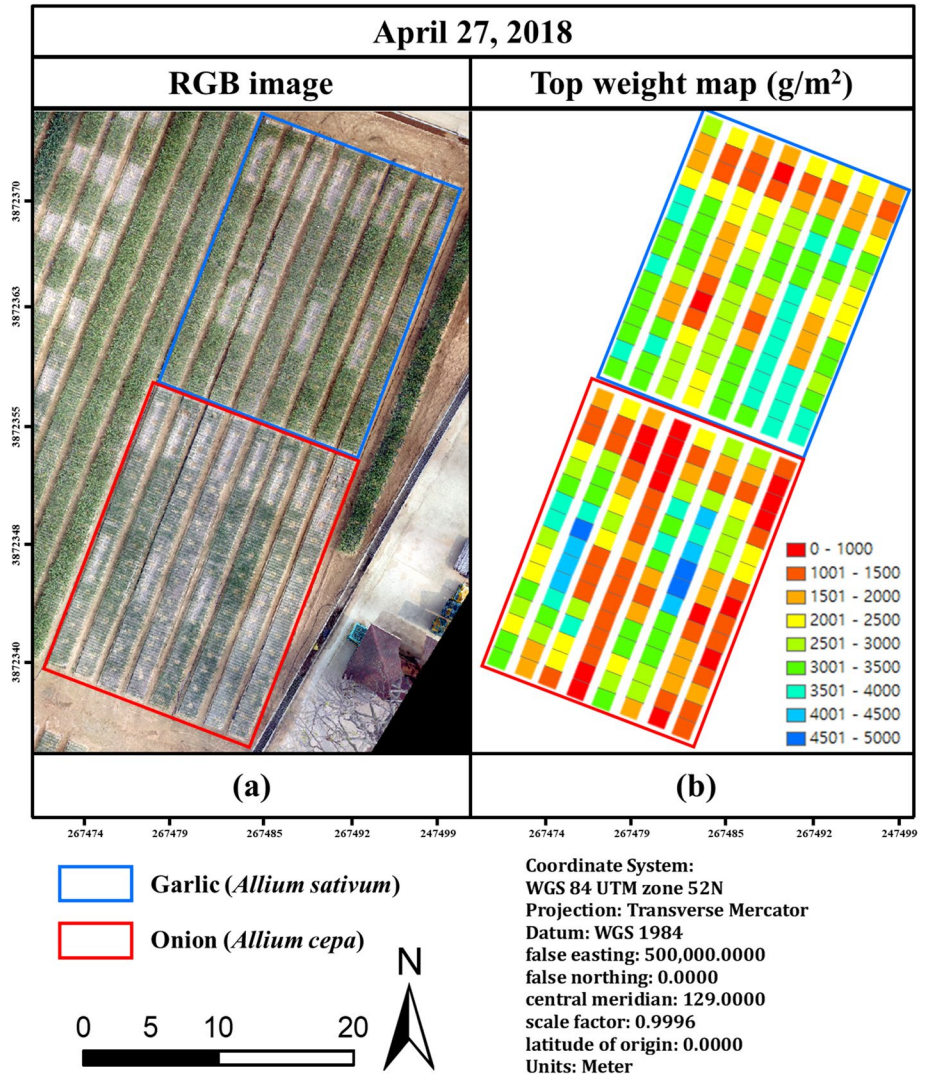

Fig. 10 **a** Unmanned aerial vehicle red, green, and blue (UAV RGB) image collected on April 27, 2018, and **b** top fresh weight map generated using the developed regression models for onion and garlic

generated to graphically show the spatial variability of the top fresh weights of each ROI, which ranged from 0 to 5000 g/m^2 for onion and from 0 to 4000 g/m^2 for garlic.

The vegetation proportion of both crops in the fields appeared to vary in the RGB image (Fig. 10a) meaning that various fresh weights could be expected depending on location. For example, crop sampling areas or areas with low crop growth were expressed in red, and areas where crops grew well were expressed in green to blue colors so that the degree of crop growth could be evaluated by location. Thus, using the yield map allowed for useful analyses, and the fresh weight maps created with the UAV

RGB imagery, together with the developed growth models, could be used to assess the potential yields of the two crops based on their location before harvest.

Conclusions

In this study, a crop segmentation algorithm based on the a* band in the CIE L*a*b* color space and MS algorithm was developed to extract onion and garlic from complex backgrounds including plastic mulch, soil, and shadows under Korean cultivation conditions. Consequently, compared to ExG and Otsu's thresholding, the a* band + MS algorithm provided an improved ability to calculate the VF of onion and garlic, which are crops with narrow and long leaves. In addition, multiple linear regression models were developed to quantify the top and root fresh weights of onion and garlic, using the developed method (a* band + MS algorithm). The results revealed that the developed algorithm enabled a more accurate and robust crop segmentation and exhibited improved model performance for crops with long narrow leaves. The validation results confirmed that the UAV RGB images processed applying the developed algorithm can be used to quantify the spatial and temporal variability of onion and garlic growth parameters.

This research differs from previous studies in the following ways: (1) A CIE L*a*b* color space and region-based MS algorithm were employed to separate crops with long narrow leaves from a complex background common under Korean field conditions; (2) a two-year field experiment was conducted to investigate the applicability of the developed segmentation algorithm and regression models and (3) this UAV RGB system can evaluate the potential yield of the crops before harvest by generating a yield map for the comparative analysis of the fresh weights of onion and garlic.

In terms of commercial setting, this study presented a series of image processing procedures including several image pre-processing techniques (i.e., image geo-referencing, radiometric calibration, and two-point normalization) to reduce errors when the developed algorithm is applied to a large area. The geo-referencing technique based on GCP enabled accurate image orthomosaic and spatial mapping without positional errors in a large area. The radiometric calibration technique based on the calibration targets minimized the influence of the weather so that normalized reflectance images could be obtained on any day of the experiment. The two-point normalization improved the estimation accuracy by compensating the slope and offset of the validation result using the two actual values. In this study, the application possibility of spatial and temporal growth mapping of onion and garlic in a large commercial field was evaluated by applying the proposed image procedure to a two-year experiment. In addition, the developed algorithms can be applied to various crops with long narrow leaves, such as green onion as well as onion and garlic. If data for growth modeling can be obtained, growth mapping can be performed for various crops in a similar environment.

Acknowledgements This research was supported by the Korea Institute of Planning and Evaluation for Technology in Food, Agriculture, Forestry, and Fisheries (Project Number: 315011-03-1-SB010, and 322032-3), Republic of Korea.

Declarations

Conflict of interest The authors declare no conflict of interest.

References

Ammour, N., Alhichri, H., Bazi, Y., Benjdira, B., Alajlan, N., & Zuair, M. (2017). Deep learning approach for car detection in UAV imagery. *Remote Sensing, 9*(4), 312. https://doi.org/10.3390/rs9040312

Bai, X., Cao, Z., Wang, Y., Yu, Z., Hu, Z., Zhang, X., & Li, C. (2014). Vegetation segmentation robust to illumination variations based on clustering and morphology modelling. *Biosystems Engineering, 125*, 80–97. https://doi.org/10.1016/j.biosystemseng.2014.06.015

Bai, Y., Nie, C., Wang, H., Cheng, M., Liu, S., Yu, X., Shao, M., Wang, Z., Wang, S., & Tuohuti, N. (2022). A fast and robust method for plant count in sunflower and maize at different seedling stages using high-resolution UAV RGB imagery. *Precision Agriculture, 23*(5), 1720–1742. https://doi.org/10.1007/s11119-022-09907-1

Borchard, N., Schirrmann, M., von Hebel, C., Schmidt, M., Baatz, R., Firbank, L., Vereecken, H., & Herbst, M. (2015). Spatio-temporal drivers of soil and ecosystem carbon fluxes at field scale in an upland grassland in Germany. *Agriculture, Ecosystems & Environment, 211*, 84–93. https://doi.org/10.1016/j.agee.2015.05.008

Bu, R., Xiong, J., Chen, S., Zheng, Z., Guo, W., Yang, Z., & Lin, X. (2020). A shadow detection and removal method for fruit recognition in natural environments. *Precision Agriculture, 21*, 782–801. https://doi.org/10.1007/s11119-019-09695-1

Chang, A., Eo, Y., Kim, S., Kim, Y., & Kim, Y. (2011). Canopy-cover thematic-map generation for Military Map products using remote sensing data in inaccessible areas. *Landscape and Ecological Engineering, 7*(2), 263–274. https://doi.org/10.1007/s11355-010-0132-1

Cheng, Y. (1995). Mean shift, mode seeking, and clustering. *IEEE Transactions on Pattern Analysis and Machine Intelligence, 17*(8), 790–799. https://doi.org/10.1109/34.400568

Costa, L., McBreen, J., Ampatzidis, Y., Guo, J., Gahrooei, M. R., & Babar, M. A. (2022). Using UAV-based hyperspectral imaging and functional regression to assist in predicting grain yield and related traits in wheat under heat-related stress environments for the purpose of stable yielding genotypes. *Precision Agriculture*. https://doi.org/10.1007/s11119-021-09852-5

Dammer, K. H., Thöle, H., Volk, T., & Hau, B. (2009). Variable-rate fungicide spraying in real time by combining a plant cover sensor and a decision support system. *Precision Agriculture, 10*(5), 431–442. https://doi.org/10.1007/s11119-008-9088-7

Escarabajal-Henarejos, D., Molina-Martínez, J., Fernández-Pacheco, D., & García-Mateos, G. (2015). Methodology for obtaining prediction models of the root depth of lettuce for its application in irrigation automation. *Agricultural Water Management, 151*, 167–173. https://doi.org/10.1016/j.agwat.2014.10.012

Fei, S., Hassan, M. A., Xiao, Y., Su, X., Chen, Z., Cheng, Q., Duan, F., Chen, R., & Ma, Y. (2023). UAV-based multi-sensor data fusion and machine learning algorithm for yield prediction in wheat. *Precision Agriculture*, *24*, 187–212. https://doi.org/10.1007/s11119-022-09938-8

Fernández-Pacheco, D. G., Escarabajal-Henarejos, D., Ruiz-Canales, A., Conesa, J., & Molina-Martínez, J. M. (2014). A digital image-processing-based method for determining the crop coefficient of lettuce crops in the southeast of Spain. *Biosystems Engineering, 117*, 23–34. https://doi.org/10.1016/j.biosystemseng.2013.07.014

Hamuda, E., Mc Ginley, B., Glavin, M., & Jones, E. (2017). Automatic crop detection under field conditions using the HSV colour space and morphological operations. *Computers and Electronics in Agriculture, 133*, 97–107. https://doi.org/10.1016/j.compag.2016.11.021

Hernández-Hernández, J. L., García-Mateos, G., González-Esquiva, J., Escarabajal-Henarejos, D., Ruiz-Canales, A., & Molina-Martínez, J. M. (2016). Optimal color space selection method for plant/soil segmentation in agriculture. *Computers and Electronics in Agriculture, 122*, 124–132. https://doi.org/10.1016/j.compag.2016.01.020

Holman, F. H., Riche, A. B., Michalski, A., Castle, M., Wooster, M. J., & Hawkesford, M. J. (2016). High throughput field phenotyping of wheat plant height and growth rate in field plot trials using UAV based remote sensing. *Remote Sensing, 8*(12), 1031. https://doi.org/10.3390/rs8121031

Hong, A.-X., Chen, G., Li, J.-L., Chi, Z.-R., & Zhang, D. (2004). A flower image retrieval method based on ROI feature. *Journal of Zhejiang University-Science A, 5*(7), 764–772. https://doi.org/10.1631/jzus.2004.0764

Hunt, E. R., Cavigelli, M., Daughtry, C. S., Mcmurtrey, J. E., & Walthall, C. L. (2005). Evaluation of digital photography from model aircraft for remote sensing of crop biomass and nitrogen status. *Precision Agriculture, 6*(4), 359–378. https://doi.org/10.1007/s11119-005-2324-5

Hunt, E. R., Hively, W. D., Fujikawa, S. J., Linden, D. S., Daughtry, C. S., & McCarty, G. W. (2010). Acquisition of NIR-green-blue digital photographs from unmanned aircraft for crop monitoring. *Remote Sensing, 2*(1), 290–305. https://doi.org/10.3390/rs2010290

Kim, D. W., Yun, H. S., Jeong, S. J., Kwon, Y. S., Kim, S. G., Lee, W. S., & Kim, H. J. (2018). Modeling and testing of growth status for Chinese cabbage and white radish with UAV-based RGB imagery. *Remote Sensing, 10*(4), 563. https://doi.org/10.3390/rs10040563

Kim, H. J., Sudduth, K. A., Hummel, J. W., & Drummond, S. T. (2013). Validation testing of a soil macronutrient sensing system. *Transactions of the ASABE, 56*(1), 23–31. https://doi.org/10.13031/2013.42582

Lancashire, P. D., Bleiholder, H., Boom, T. V. D., Langelüddeke, P., Stauss, R., Weber, E., & Witzenberger, A. (1991). A uniform decimal code for growth stages of crops and weeds. *Annals of Applied Biology, 119*(3), 561–601. https://doi.org/10.1111/j.1744-7348.1991.tb04895.x

Liu, S., Yin, D., Feng, H., Li, Z., Xu, X., Shi, L., & Jin, X. (2022). Estimating maize seedling number with UAV RGB images and advanced image processing methods. *Precision Agriculture, 23*(5), 1604–1632. https://doi.org/10.1007/s11119-022-09899-y

Lopez-Bellido, F. J., Lopez-Bellido, R. J., Muñoz-Romero, V., Fernandez-Garcia, P., & Lopez-Bellido, L. (2016). New phenological growth stages of garlic (*Allium sativum*). *Annals of Applied Biology, 169*(3), 423–439. https://doi.org/10.1111/aab.12312

Łuszczkiewicz-Piątek, M. (2014). Which color space should be chosen for robust color image retrieval based on mixture modeling. In *Image processing and communications challenges 5* (pp. 55–64). Springer. https://doi.org/10.1007/978-3-319-01622-1_7

Meyer, G. E., Hindman, T. W., & Laksmi, K. (1999). Machine vision detection parameters for plant species identification. In *Precision agriculture and biological quality* (Vol. 3543, pp. 327–335). International Society for Optics and Photonics. https://doi.org/10.1117/12.336896

Osco, L. P., Nogueira, K., Marques Ramos, A. P., Faita Pinheiro, M. M., Furuya, D. E. G., Gonçalves, W. N., de Castro Jorge, L. A., Marcato Junior, J., & dos Santos, J. A. (2021). Semantic segmentation of citrus-orchard using deep neural networks and multispectral UAV-based imagery. *Precision Agriculture, 22*(4), 1171–1188. https://doi.org/10.1007/s11119-020-09777-5

Otsu, N. (1979). A threshold selection method from gray-level histograms. *IEEE Transactions on Systems, Man, and Cybernetics, 9*(1), 62–66. https://doi.org/10.1109/TSMC.1979.4310076

Riehle, D., Reiser, D., & Griepentrog, H. W. (2020). Robust index-based semantic plant/background segmentation for RGB-images. *Computers and Electronics in Agriculture, 169*, 105201. https://doi.org/10.1016/j.compag.2019.105201

Salamí, E., Barrado, C., & Pastor, E. (2014). UAV flight experiments applied to the remote sensing of vegetated areas. *Remote Sensing, 6*(11), 11051–11081. https://doi.org/10.3390/rs61111051

Sarkate, R. S., Kalyankar, N., & Khanale, P. (2013). Application of computer vision and color image segmentation for yield prediction precision. In *2013 international conference on information systems and computer networks* (pp. 9–13). IEEE. https://doi.org/10.1109/ICISCON.2013.6524164

Shao, M., Nie, C., Cheng, M., Yu, X., Bai, Y., Ming, B., Song, H., & Jin, X. (2022). Quantifying effect of tassels on near-ground maize canopy RGB images using deep learning segmentation algorithm. *Precision Agriculture*. https://doi.org/10.1007/s11119-021-09842-7

Thorp, K., Wang, G., West, A., Moran, M., Bronson, K., White, J., & Mon, J. (2012). Estimating crop biophysical properties from remote sensing data by inverting linked radiative transfer and ecophysiological models. *Remote Sensing of Environment, 124*, 224–233. https://doi.org/10.1016/j.rse.2012.05.013

Torres-Sánchez, J., López-Granados, F., & Pena, J. M. (2015). An automatic object-based method for optimal thresholding in UAV images: Application for vegetation detection in herbaceous crops. *Computers and Electronics in Agriculture, 114*, 43–52. https://doi.org/10.1016/j.compag.2015.03.019

Torres-Sánchez, J., Pena, J. M., de Castro, A. I., & López-Granados, F. (2014). Multi-temporal mapping of the vegetation fraction in early-season wheat fields using images from UAV. *Computers and Electronics in Agriculture, 103*, 104–113. https://doi.org/10.1016/j.compag.2014.02.009

Tu, S., Pang, J., Liu, H., Zhuang, N., Chen, Y., Zheng, C., Wan, H., & Xue, Y. (2020). Passion fruit detection and counting based on multiple scale faster R-CNN using RGB-D images. *Precision Agriculture, 21*, 1072–1091. https://doi.org/10.1007/s11119-020-09709-3

Turner, D., Lucieer, A., & Watson, C. (2012). An automated technique for generating georectified mosaics from ultra-high resolution unmanned aerial vehicle (UAV) imagery, based on structure from motion (SfM) point clouds. *Remote Sensing, 4*(5), 1392–1410. https://doi.org/10.3390/rs4051392

Valente, J., Sari, B., Kooistra, L., Kramer, H., & Mücher, S. (2020). Automated crop plant counting from very high-resolution aerial imagery. *Precision Agriculture, 21*, 1366–1384. https://doi.org/10.1007/s11119-020-09725-3

Woebbecke, D. M., Meyer, G. E., Von Bargen, K., & Mortensen, D. A. (1995). Color indices for weed identification under various soil, residue, and lighting conditions. *Transactions of the ASAE, 38*(1), 259–269. https://doi.org/10.13031/2013.27838

Xu, L., Zhou, L., Meng, R., Zhao, F., Lv, Z., Xu, B., Zeng, L., Yu, X., & Peng, S. (2022). An improved approach to estimate ratoon rice aboveground biomass by integrating UAV-based spectral, textural and structural features. *Precision Agriculture, 23*(4), 1276–1301. https://doi.org/10.1007/s11119-022-09884-5

Yan, W., Guan, H., Cao, L., Yu, Y., Li, C., & Lu, J. (2020). A self-adaptive mean shift tree-segmentation method using UAV LiDAR data. *Remote Sensing, 12*(3), 515. https://doi.org/10.3390/rs12030515

Zhang, C., & Kovacs, J. M. (2012). The application of small unmanned aerial systems for precision agriculture: A review. *Precision Agriculture, 13*(6), 693–712. https://doi.org/10.1007/s11119-012-9274-5

Zheng, L., Zhang, J., & Wang, Q. (2009). Mean-shift-based color segmentation of images containing green vegetation. *Computers and Electronics in Agriculture, 65*(1), 93–98. https://doi.org/10.1016/j.compag.2008.08.002

Authors and Affiliations

Dong-Wook Kim[1,2] · Sang Jin Jeong[1] · Won Suk Lee[3] · Heesup Yun[4] · Yong Suk Chung[5] · Young-Seok Kwon[6] · Hak-Jin Kim[1,2,7]

1 Department of Biosystems Engineering, College of Agriculture and Life Sciences, Seoul National University, Seoul, Republic of Korea

2 Research Institute of Agriculture and Life Sciences, Seoul National University, Seoul, Republic of Korea

3 Department of Agricultural and Biological Engineering, University of Florida, Gainesville, FL, USA

4 Department of Biological and Agricultural Engineering, University of California Davis, Davis, CA, USA

5 Department of Plant Resources and Environment, Jeju National University, Jeju, Republic of Korea

6 Department of Horticultural Crop Research, National Institute of Horticultural and Herbal Science, Muan, Republic of Korea

7 Integrated Major in Global Smart Farm, College of Agriculture and Life Sciences, Seoul National University, Seoul, Republic of Korea